Monthly Notices
of the
ROYAL ASTRONOMICAL SOCIETY

MNRAS **465,** 739–745 (2017)
Advance Access publication 2016 October 27

doi:10.1093/mnras/stw2753

When does an old nova become a dwarf nova? Kinematics and age of the nova shell of the dwarf nova AT Cancri

Michael M. Shara,[1]★† Laurent Drissen,[2] Thomas Martin,[2] Alexandre Alarie[2] and F. Richard Stephenson[3]

[1]*Department of Astrophysics, American Museum of Natural History, Central Park West at 79th Street, New York, NY 10024-5192, USA*
[2]*Département de physique, de génie physique et d'optique, Université Laval, Québec (QC) G1V 0A6, Canada*
[3]*Department of Physics, Durham University, South Road, Durham DH1 3LE, UK*

Accepted 2016 October 21. Received 2016 October 20; in original form 2016 September 16

ABSTRACT

The Z Cam-type dwarf nova AT Cancri (AT Cnc) displays a classical nova (CN) shell, demonstrating that mass transfer in cataclysmic binaries decreases substantially after a CN eruption. The hibernation scenario of cataclysmic binaries predicts such a decrease, on a timescale of a few centuries. In order to measure the time since AT Cnc's last CN eruption, we have measured the radial velocities of a hundred clumps in its ejecta with SITELLE, Canada–France–Hawaii Telescope's recently commissioned imaging Fourier transform spectrometer. These range from −455 to +490 km s^{-1}. Coupled with the known distance to AT Cnc of 460 pc, the size of AT Cnc's shell, and a simple model of nova ejecta deceleration, we determine that the last CN eruption of this system occurred 330^{+135}_{-90} yr ago. This is the most rapid transition from a high mass-transfer rate, nova-like variable to a low mass-transfer rate, dwarf nova yet measured, and in accord with the hibernation scenario of cataclysmic binaries. We conclude by noting the similarity in the deduced outburst date (within a century of 1686 CE) of AT Cnc to a 'guest star' reported in the constellation Cancer by Korean observers in 1645 CE.

Key words: techniques: imaging spectroscopy – stars: individual: AT Cnc – novae, cataclysmic variables – ISM: jets and outflows.

1 INTRODUCTION

Dwarf novae (DNe) and classical novae (CNe) are binary stars, wherein a white dwarf (WD) accretes hydrogen-rich matter from a companion. That companion is a red dwarf (RD), filling its Roche lobe in the case of a DN; it is an RD or a red giant in the case of a CN. In DNe, a thermal instability episodically dumps much of the accretion disc on to the WD (Osaki 1974). The liberation of gravitational potential energy then brightens these systems by up to 100-fold as DN eruptions occur, typically every few weeks or months. This accretion process in DNe must inevitably build an electron degenerate, hydrogen-rich envelope on the WD (Shara et al. 1986). Theory and detailed simulations predict that once the accreted mass reaches of the order of 10^{-5} M$_\odot$, a thermonuclear runaway (TNR) will occur in the degenerate layer of accreted hydrogen (Starrfield et al. 1972; Prialnik, Shara & Shaviv 1978). The TNR causes the rapid rise to $\sim 10^5$ L$_\odot$ or more, and the high-speed ejection of the accreted envelope in a CN explosion.

The long-term evolution of cataclysmic binaries (CBs) is driven by the mass-accretion rate between nova eruptions. If that rate decreases by one or more orders of magnitude in the centuries following a CN eruption, as predicted by the hibernation scenario of CBs (Prialnik & Shara 1986; Shara et al. 1986; Kovetz, Prialnik & Shara 1987), then the predicted relative numbers of long- and short-period CBs, the relative numbers of DNe and nova-like binaries, and the lifetimes of CBs all change dramatically. Population synthesis codes that model CBs and their effects on the chemical evolution of galaxies (Matteucci et al. 2003; Chen et al. 2016) can provide only realistic predictions if accurate mass-transfer rate histories are an inherent part of those codes.

The accretion rates on to the WDs in DNe are typically 10–100 times smaller than those observed in the WD–RD, mass-transferring binaries known as nova-like variables. Collazzi et al. (2009) demonstrated that almost all pre- and post-nova binaries, observed in the century before or after an eruption, are high mass-transfer rate nova-like variables. Thus, the discovery of a CN shell, almost 1° in diameter, surrounding the prototypical DN Z Cam (Shara et al. 2007) was unexpected, and has important implications for our understanding of the long-term evolution of CBs. The

★ E-mail: mshara@amnh.org
† This paper is respectfully dedicated to the memory of Peter Wehinger, co-discoverer of AT Cancri's ejecta, who selflessly devoted much of his professional life to the advancement of astronomy.

derived shell mass of Z Cam matches that of CNe, and is inconsistent with the mass expected from a DN wind or a planetary nebula. The Z Cam shell observationally linked, for the first time, a prototypical DN with an ancient CN eruption and the CN process. This was the first-ever confirmation of a key prediction of CB TNR theory: The accreting WDs in DNe must eventually erupt as CNe. It also demonstrated that, 1300–2100 yr after its CN eruption (Shara et al. 2012a), Z Cam's central binary is *not* a nova-like variable. Instead, it exhibits DN eruptions, indicative of a lower mass-transfer rate than is seen in old novae up to one century after eruption. The hibernation scenario of CBs predicts that the transition from a high to low mass-transfer state in old novae is just the WD cooling time after a CN eruption – a few centuries. A nova that erupted more recently than Z Cam is required to more stringently test the predicted transition time-scale.

Thus motivated, we have been searching for other CN shells surrounding DNe. One of our targets was the Z Cam-like DN AT Cancri (AT Cnc). Short- and long-term variability in the spectrum of AT Cnc has been well documented by Nogami et al. (1999), and references therein, who detected a clear radial velocity variation with a period of 0.2011 d, a semi-amplitude of 80 km^{-1}, and a systemic velocity of 11 km s^{-1}. Superhumps were detected by Kozhevnikov (2004), who suggested that AT Cnc has a large mass ratio, and may host a magnetic WD.

Optical [N II] narrow-band imaging of AT Cnc (Shara et al. 2012b) revealed highly fragmented rings, about 3 arcmin in diameter, surrounding the star. The spectrum of one of the brightest blobs in the ejecta is dominated by lines of [N II], [O II], and [O III]; oxygen and nitrogen are the products of a nova TNR. The geometry of the rings suggests that we are looking at an hourglass-shaped ejection reminiscent of that of other old novae such as HR Del (Harman & O'Brien 2003).

We present in this paper a kinematical analysis of a hundred emission-line blobs around AT Cnc, based on a hyperspectral data cube obtained with the Canada–France–Hawaii Telescope's newly commissioned imaging Fourier transform spectrometer (iFTS), SITELLE. The key aim of this study is to use the kinematics of the ejecta as a clock, to determine the time since AT Cnc's last eruption. We briefly describe SITELLE in Section 2, and the observations of AT Cnc and their reductions in Section 3. The results are presented, and the time since the last CN eruption of AT Cnc is deduced, in Section 4. We summarize our results in Section 5. The spectrum of AT Cnc and a discussion of its possible association with the Korean 'guest star' of 1645 CE are given in appendices.

2 DESCRIPTION OF THE INSTRUMENT

As the instrument used to collect the data presented in this paper is new and unusual, and since this is one of the first science papers using SITELLE data, a brief introduction to the instrument is given here. SITELLE[1] is essentially an imager, at the core of which a Michelson interferometer is inserted in order to modulate the incoming light and extract the spatially resolved spectral content of its target. The interferometer consists of a beam splitter, which separates the incoming beam into two components, one of which is sent to a fixed mirror and the other one to a moving mirror. The two beams are reflected back by these mirrors and interfere. The interferometric images are then recorded on two e2v 2048 × 2048 pixel CCDs. This is enabled by an unusual mirror configuration permitting one of the two output beams to be reflected at an angle with respect to the incoming beam (in a standard Michelson interferometer, this beam is reflected back to the source). Moving one of the mirrors introduces an optical path difference (OPD) between the two arms of the interferometer, modulating the light according to the spectral content of the source at each location in the field of view. A series of short (10–100 s) images are acquired by both CCDs at different regularly spaced mirror positions, resulting in two complementary interferometric cubes, which are then combined. Each pixel (0.32 arcsec) in the image plane records an interferogram, which, after proper data processing, is transformed into a spectrum. The net result of a SITELLE observation is thus a spatially resolved spectral cube of the target, with a field of view of 11 arcmin and a seeing-limited spatial resolution sampled at 0.32 arcsec.

The cube's spectral resolution depends on the maximum OPD between the mirrors, and therefore the number of mirror steps, which is tailored to the observer's needs. Typical spectral resolutions vary from $R \sim 500$ to 2000, although the instrument is capable of reaching $R \sim 10\,000$. It has been tested and shown to work on astronomical sources up to $R \sim 5000$. In order to obtain the desired spectral resolution in a reasonable amount of time while reducing the background photon noise, filters are inserted in the optical path. More details about SITELLE, its metrology system, and its performances are given in Grandmont et al. (2012), Drissen et al. (2014), and Brousseau et al. (2014).

[1] http://cfht.hawaii.edu/Instruments/Sitelle/

3 OBSERVATIONS AND DATA REDUCTION

AT Cnc was observed on 2016 January 9, as part of SITELLE's Science Verification phase using the SN3 filter (flat transmission above 95 per cent in the 651–685 nm range) at a spectral resolution of $R = 1300$. This spectral region contains the three strongest lines in the optical part of the ejecta spectrum, due to [N II] and Hα. We note that these spectra were not intended for, and are not useful for abundance analyses, as the ejecta of AT Cnc have swept up a mass of interstellar medium (ISM) that is several times larger than the original ejecta mass. They are, however, powerful probes of the kinematics and age of the ejecta.

To reach the $R = 1300$ resolution, 232 equally spaced mirror steps of 2881 nm each were necessary, with an integration time of 57 s per step and an overhead (CCD readout and mirror displacement) of 3.8 s per step, for a total observation time of 3.9 h. The sky was moonless and photometric, with an average seeing of 0.95 arcsec. The data were reduced using ORBS, SITELLE's dedicated data reduction software (Martin, Drissen & Joncas 2015; Martin, Prunet & Drissen 2016).

Fig. 1 shows the deep image of the field, obtained by summing all interferograms. As was already noted in Shara et al. (2012b), the ejecta are very asymmetrically distributed about AT Cnc, with the majority of the blobs located to its north-west, north, east, and south-east. Almost no blobs are seen to AT Cnc's south-west. A possible explanation for this asymmetry is connected to the observation that only ∼47 per cent of old novae display ejected shells (Cohen 1985; Downes & Duerbeck 2000). Shock interaction with the surrounding ISM is essential to excite the forbidden nitrogen lines that provide the strongest emission lines seen in most old nova ejecta. Novae with no detectable ejected shells may simply lie in regions of low ISM. If the ISM surrounding AT Cnc is significantly denser to the north and east, then the asymmetry in the ejecta is easily understood.

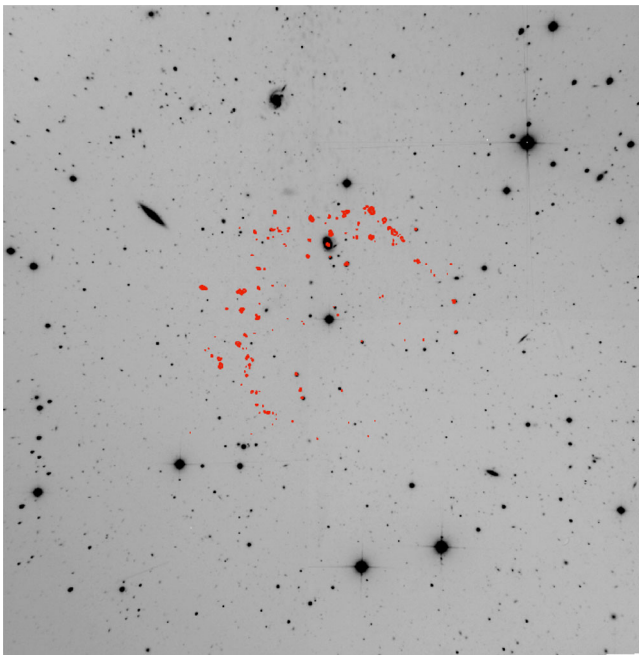

Figure 1. Deep image of the entire field of view, with contours (in red) of the most prominent emission-line blobs around AT Cnc. The field of view is 11 × 11 arcmin^2, with north at the top and east to the left. Numerous galaxies are seen in the field, some of which having redshifts that put their emission lines in the SN3 filter. They will be discussed in Drissen et al. (in preparation).

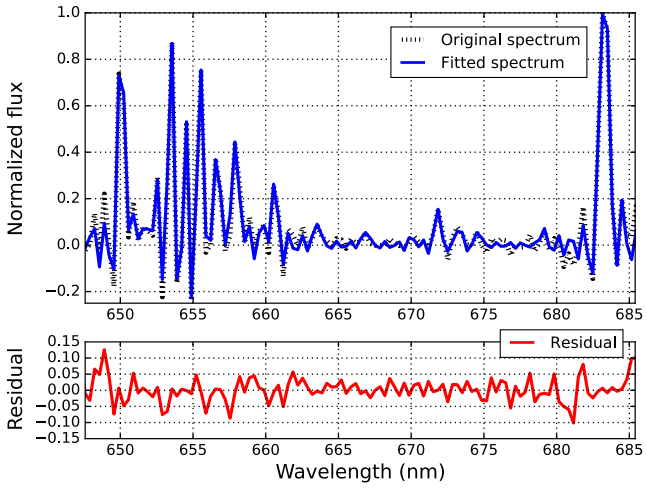

Figure 2. Average observed spectrum of the night sky (black) and fit to the OH lines (upper panel); residuals are shown in the lower panel.

3.1 Wavelength and flux calibration

Wavelength calibration with SITELLE is secured using a high-resolution He–Ne (543.5-nm) data cube obtained at least once during the observing run. We have noticed small zero-point offsets from one cube to the next, caused in part by the fact that the targets are observed at an angle compared with the calibration laser cube. However, cubes obtained with the SN3 filter can be calibrated with an absolute precision of about 1–3 km s^{-1}, thanks to numerous night-sky OH lines (Fig. 2) filling the entire field of view of the detector. Therefore, the uncertainties in the blobs' radial velocities are completely dominated by uncertainties in the line fitting (and thus the signal-to-noise ratio of individual spectra) rather than the instrumental zero-point.

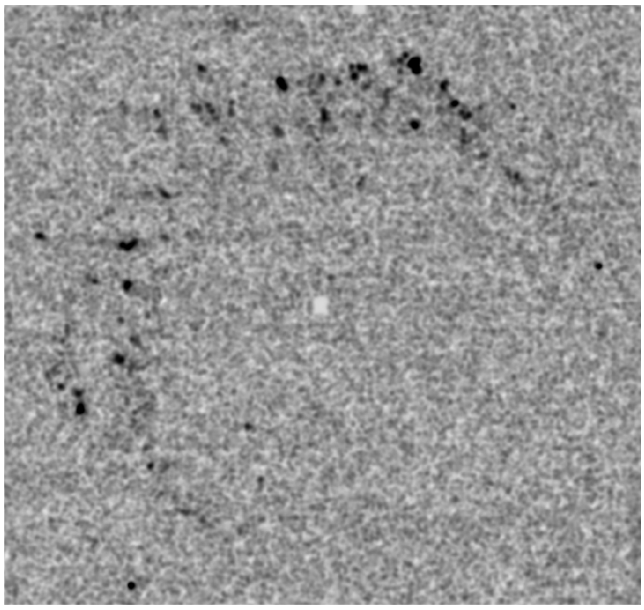

Figure 3. Frame 125 from the cube, centred at 6585 Å. The image has been convolved with a 2.5-pixel Gaussian in order to enhance the blobs' appearance over the background.

Flux calibration is obtained with regular observations of spectrophotometric standard stars during the night, tied to a data cube of the spectrophotometrically calibrated compact planetary nebula M1-71 obtained during a previous observing run. Because of possible variations of the interferometer's modulation efficiency from one night to the next, we estimate that the absolute uncertainty on the flux is of the order of 10 per cent.

3.2 Blob identification and radial velocities

Because the [N II] doublet, with its associated blueshift and redshift, falls within the night-sky OH-line forest, an average spectrum of the sky, obtained from regions in the cube without bright targets, was subtracted from the original cube before identifying the blobs. Blobs were then visually detected and identified in individual frames (see Fig. 3) of the cube. Whereas the majority of them were well defined, some were more diffuse and thus more difficult to characterize; these diffuse and faint structures are not included in the present analysis.

Spectra were extracted with SAOImage DS9, using the most appropriate aperture, given the shape and orientation of each blob. A fitting routine using the correct instrument line shape (essentially a convolution of a sinc function with a Gaussian) described in Martin et al. (2016) was then applied to each spectrum, providing radial velocities and reliable uncertainties (Table 1, where blobs are listed in increasing order of radial velocity, from the most blueshifted to the most redshifted). In 51 cases, the fainter [N II] 6548 line was clearly detected and fitted. Examples of spectra and fits are shown in Fig. 4, for the brightest and the faintest blobs in our sample. Uncertainties on radial velocities range from 2 to 28 km s^{-1} (clearly anticorrelated with the flux in the [N II] lines, as expected), with an average of 12 km s^{-1}, which is less than a tenth of a velocity channel and about 1 per cent of the global velocity range (∼1000 km s^{-1}) in the shell. A spectrum of the central star is discussed in Appendix A.

Table 1. Properties of blobs in AT Cnc.

ID	RA (J2000.0)	Dec. (J2000.0)	RV (km s^{-1})	RV error (km s^{-1})	Flux (10^{-16} erg s^{-1} cm^{-2})
1	8:28:41.37	+25:20:10.6	−455	13	2.4
2	8:28:35.88	+25:21:09.8	−438	16	1.4
3	8:28:41.78	+25:20:28.8	−436	7	4.3
4	8:28:39.83	+25:20:40.4	−432	12	2.8
5	8:28:35.90	+25:21:13.4	−403	12	2.6
6	8:28:35.15	+25:21:14.9	−400	19	1.6
7	8:28:40.75	+25:21:16.6	−343	19	0.9
8	8:28:42.82	+25:19:48.5	−341	16	1.6
9	8:28:43.18	+25:19:46.9	−340	16	1.3
10	8:28:43.24	+25:20:25.8	−335	9	3.2
11	8:28:40.07	+25:21:28.1	−324	19	1.0
12	8:28:41.98	+25:21:04.2	−320	10	5.2
13	8:28:42.48	+25:21:06.5	−311	8	4.1
14	8:28:42.77	+25:20:41.0	−318	9	1.8
15	8:28:40.91	+25:21:23.7	−286	9	3.3
16	8:28:44.09	+25:20:10.1	−278	15	2.5
17	8:28:41.34	+25:21:23.2	−209	10	2.7
18	8:28:45.93	+25:20:33.8	−158	6	4.9
19	8:28:32.36	+25:21:36.1	−158	11	1.5
20	8:28:44.07	+25:19:00.7	−156	12	1.4
21	8:28:46.15	+25:20:35.4	−146	2	15.6
22	8:28:41.75	+25:18:33.4	−142	12	1.7
23	8:28:40.80	+25:18:26.4	−120	16	1.0
24	8:28:41.87	+25:18:38.9	−101	17	0.6
25	8:28:41.56	+25:18:31.7	−100	9	1.4
26	8:28:32.22	+25:21:27.6	−98	6	2.5
27	8:28:41.59	+25:18:32.1	−97	11	4.0
28	8:28:40.79	+25:21:48.7	−87	9	4.4
29	8:28:32.86	+25:21:39.4	−83	5	4.5
30	8:28:32.11	+25:21:25.3	−72	8	3.6
31	8:28:32.48	+25:21:31.2	−34	6	3.4
32	8:28:44.88	+25:19:18.7	−35	5	2.7
33	8:28:35.60	+25:21:48.4	−30	12	2.5
34	8:28:34.29	+25:21:46.2	−30	15	1.1
35	8:28:30.48	+25:20:58.8	−30	7	2.2
36	8:28:45.52	+25:19:27.9	−30	9	1.6
37	8:28:35.43	+25:21:48.0	−26	15	1.6
38	8:28:36.82	+25:21:43.7	−25	12	2.2
39	8:28:44.35	+25:20:14.4	−25	14	1.3
40	8:28:35.75	+25:21:44.2	−23	11	3.0
41	8:28:44.89	+25:19:17.1	−17	4	5.2
42	8:28:36.30	+25:21:41.4	−10	11	2.1
43	8:28:34.73	+25:21:36.8	−5	15	1.5
44	8:28:44.93	+25:19:24.6	−5	12	3.9
45	8:28:35.39	+25:21:39.2	−2	18	1.1
46	8:28:42.62	+25:18:52.4	−1	10	1.6
47	8:28:40.47	+25:21:29.5	0	13	1.8
48	8:28:33.73	+25:21:46.7	1	4	7.6
49	8:28:38.21	+25:21:42.4	5	5	5.0
50	8:28:33.80	+25:21:50.0	11	2	19.1
51	8:28:34.09	+25:21:52.9	13	13	1.9
52	8:28:34.26	+25:21:51.0	14	14	1.2
53	8:28:31.55	+25:21:08.4	14	14	1.7
54	8:28:43.51	+25:19:57.4	16	17	0.6
55	8:28:45.43	+25:19:48.3	18	18	0.9
56	8:28:32.23	+25:21:17.2	22	14	3.4
57	8:28:38.09	+25:21:39.7	29	6	3.6
58	8:28:40.13	+25:21:16.8	35	15	1.5
59	8:28:39.80	+25:21:29.0	42	27	1.8
60	8:28:38.31	+25:21:19.4	46	11	3.3
61	8:28:43.19	+25:19:35.9	43	14	1.9
62	8:28:43.63	+25:19:07.5	55	7	6.7
63	8:28:40.54	+25:21:32.1	56	17	0.7
64	8:28:43.30	+25:20:12.6	56	6	4.5
65	8:28:43.09	+25:19:16.4	60	14	0.8
66	8:28:40.85	+25:21:30.9	68	13	1.7
67	8:28:35.86	+25:21:48.4	68	9	1.5
68	8:28:43.19	+25:19:19.4	82	14	0.9
69	8:28:43.16	+25:20:30.4	88	5	9.0
70	8:28:39.80	+25:21:33.3	101	15	1.1
71	8:28:36.79	+25:21:26.5	103	6	3.6
72	8:28:42.11	+25:20:53.5	106	8	5.0
73	8:28:42.31	+25:21:29.5	108	10	1.5
74	8:28:43.45	+25:20:30.7	112	5	3.8
75	8:28:35.65	+25:21:26.0	115	13	1.5
76	8:28:38.44	+25:21:04.8	116	10	2.0
77	8:28:36.84	+25:21:29.5	124	10	1.8
78	8:28:33.83	+25:21:22.4	140	3	13.7
79	8:28:42.18	+25:18:54.2	145	22	0.8
80	8:28:42.98	+25:19:08.3	148	10	1.8
81	8:28:42.27	+25:18:39.0	149	10	4.6
82	8:28:42.08	+25:20:34.7	157	8	2.0
83	8:28:42.80	+25:19:19.3	157	9	2.5
84	8:28:42.72	+25:19:12.8	161	15	1.0
85	8:28:42.51	+25:19:22.8	162	8	4.3
86	8:28:41.05	+25:20:35.5	174	10	0.8
87	8:28:31.61	+25:21:21.0	177	9	3.5
88	8:28:42.05	+25:19:52.6	183	12	4.1
89	8:28:42.69	+25:19:16.0	183	15	2.2
90	8:28:42.33	+25:18:51.3	184	10	2.1
91	8:28:42.84	+25:19:27.1	188	9	2.7
92	8:28:42.25	+25:20:06.9	189	9	2.8
93	8:28:42.24	+25:18:46.8	196	18	2.0
94	8:28:42.39	+25:19:49.7	202	10	2.4
95	8:28:36.92	+25:21:16.5	212	12	6.4
96	8:28:34.84	+25:21:22.0	217	11	3.7
97	8:28:42.77	+25:19:33.9	238	15	1.4
98	8:28:40.38	+25:20:37.0	264	15	1.3
99	8:28:40.17	+25:20:36.6	290	10	3.1
100	8:28:42.14	+25:20:04.9	293	4	10.8
101	8:28:38.80	+25:19:58.4	297	9	1.5
102	8:28:38.96	+25:20:00.1	311	10	2.2
103	8:28:39.10	+25:18:54.3	385	8	2.4
104	8:28:33.03	+25:20:24.6	393	10	2.0
105	8:28:32.82	+25:20:23.9	399	17	1.3
106	8:28:36.35	+25:20:06.7	401	13	2.0
107	8:28:36.09	+25:18:52.1	420	11	2.4
108	8:28:31.74	+25:19:14.6	421	18	0.8
109	8:28:33.27	+25:20:22.3	442	14	1.6
110	8:28:37.31	+25:18:32.2	448	17	1.8
111	8:28:31.84	+25:19:10.4	468	22	0.3
112	8:28:30.54	+25:19:38.4	470	18	2.4
113	8:28:34.26	+25:19:26.8	472	12	6.0
114	8:28:32.13	+25:19:08.9	480	28	0.6
115	8:28:30.16	+25:19:40.9	490	8	2.5

Table 1 – *continued*

4 THE EXPANSION AND AGE OF THE AT CNC EJECTA

4.1 Expansion

In Fig. 5, we plot the distribution of radial velocities in order of increasing values. Two sharp discontinuities are seen, between −160 and −275 km s^{-1}, and between +310 and +400 km s^{-1}. These discontinuities are likely associated with the transition from polar caps

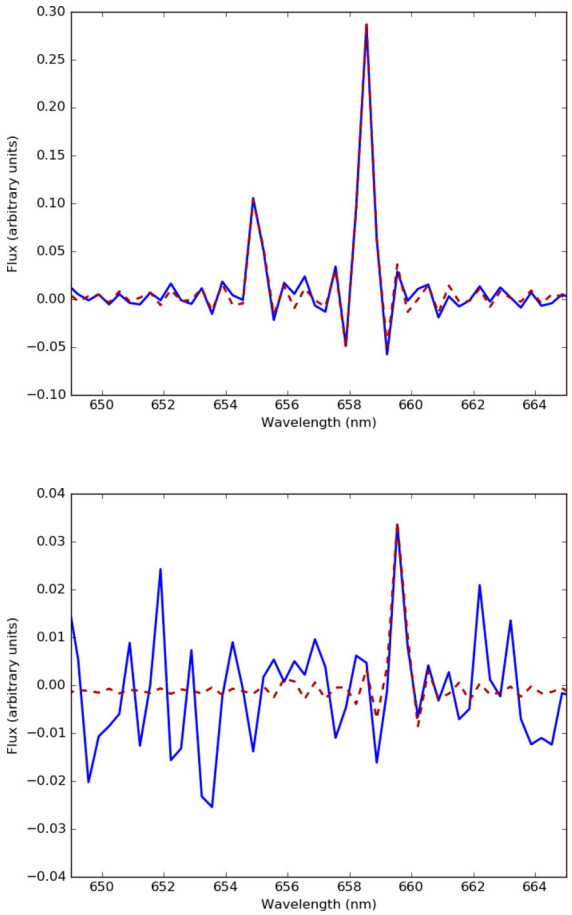

Figure 4. Spectra of blobs illustrating the quality of the fits used to determine their radial velocities in two extreme cases. Data are in solid blue, while the fits are represented by red dashed lines. The upper panel shows the spectrum of blob number 50, having the lowest uncertainty on the radial velocity (2 km s^{-1}); oscillations across the spectrum are not noise, but rather characteristic of the sinc function corresponding to an FTS instrument line function. The lower panel shows the spectrum of blob number 114, with the [N II] 6584 line barely above the noise; it has the largest uncertainty (28 km s^{-1}).

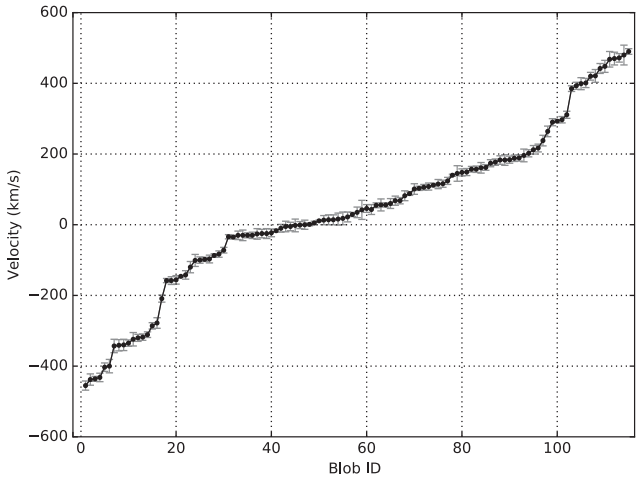

Figure 5. Distribution of radial velocities. Note the sharp discontinuities between −160 and −275 km s^{-1}, and between +310 and +400 km s^{-1}.

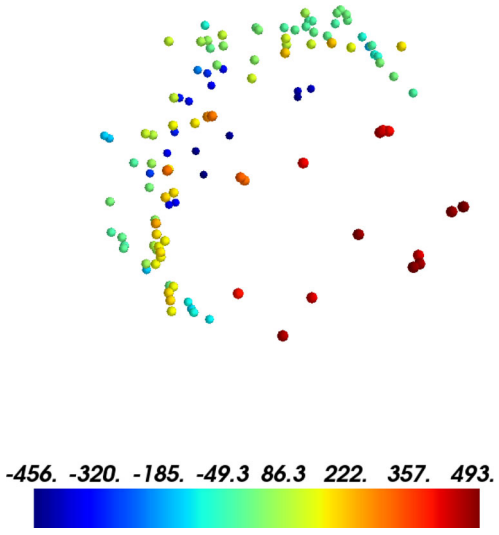

Figure 6. Excerpt from the 3D animation, showing the AT Cnc nebula in the (α, δ) plane, colour-coded according to the blobs' radial velocities. Refer to Movie 1 for an animation of these data (available in the online journal).

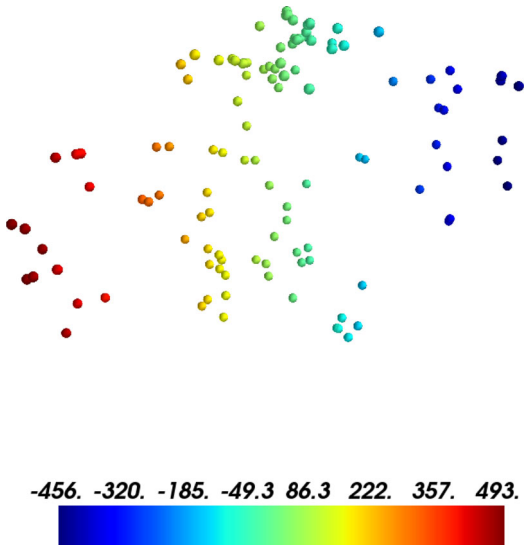

Figure 7. Excerpt from the 3D animation, showing the AT Cnc nebula in the (RV, δ) plane, colour-coded according to the blobs' radial velocities. The observer is located on the right-hand side. Refer to Movie 1 for an animation of these data (available in the online journal).

to an equatorial ring, an ejecta geometry often seen in CNe (Gill & O'Brien 1999; Harman & O'Brien 2003; Chesneau et al. 2012). The maximum projected ejection velocity observed with respect to the central star is 475 km s^{-1}. Since the distance to AT Cnc is reasonably well established at 460^{+186}_{-133} pc (Shara et al. 2012b), so is the largest projected distance of an ejecta blob, on the equatorial belt: $0.22^{+0.09}_{-0.06}$ pc.

If we assume a linear scaling factor between observed radial velocities of blobs and the projected distance from the plane of the sky containing AT Cnc, we can model the 3D distribution of the blobs. A value of 1 km s^{-1} = 1 pixel yields the 3D distribution of the blobs depicted in Figs 6 and 7. While Fig. 7 supports the suggestion that the discontinuities noted in Fig. 5 are, in fact, associated with the transition from polar caps to an equatorial ring, the scaling factor adopted above may be larger or smaller than the value adopted,

expanding or shrinking the elongation of the polar blobs with respect to the equatorial ring. Figs 6 and 7 and Movie 1 (available in the online journal) suggest that the axis joining the polar blobs is inclined at ∼30°–40° to our line of sight, so that the largest radial velocities, with respect to AT Cnc, in the polar caps would then be 15–30 per cent larger than the measured value of 475 km s^{-1}, i.e. ∼550–600 km s^{-1}.

4.2 Age

Since we cannot precisely correct for projection effects, either of the radial velocity or of the distance from AT Cnc of the most distant blobs, the simplest and most conservative approach is to adopt the maximum observed extension ($0.22^{+0.09}_{-0.06}$ pc) and the maximum observed radial velocity (475 km s^{-1}) as we estimate the time T since AT Cnc's last nova eruption. (The age estimated below increases by only a few decades if we adopt velocities and maximal distances corrected for inclination, as these tend to cancel each other.) If we ignore the deceleration of the ejecta, we find $T = 489^{+200}_{-133}$ yr.

However, nova shells *are* observed to decelerate, with ejection velocities halving on a time-scale of 75 yr (Oort 1946; Duerbeck 1987). During the initial, free-expansion phase after a nova eruption (with a time t ranging from a few years to a few decades), the ejected mass is much larger than the mass swept up from the ISM. Thus, the ejecta expand in radius R at nearly constant velocity v, so that $R \sim t$. Once the swept-up mass is larger than the ejecta mass (the 'Sedov–Taylor' phase), deceleration occurs, so that for constant interstellar matter density, one finds $R \sim t^{0.4}$ and $v \sim t^{-0.6} \sim R^{-1.5}$ (Taylor 1950). These relationships yield an initial ejection velocity from AT Cnc of 2200 km s^{-1}, which occurred 330^{+135}_{-90} yr ago. We note again that this age barely changes if we adopt inclination-corrected velocities and maximal distances (as larger velocities and distances cancel each other). This remarkably short time-scale is in excellent agreement with the prediction of the decline time of mass transfer after a nova eruption (Kovetz et al. 1987). The high deduced initial ejection velocity implies that AT Cnc was an intrinsically luminous, fast nova (Yaron et al. 2005).

As we have already noted, this young age has important implications for our understanding of the long-term evolution of CBs. While most novae which erupted in the past century are now 'nova-like variables' (Collazzi et al. 2009), transferring matter at high rates from their RDs to their WD primaries, only a handful of older novae have been identified. After 233 yr of its eruption, WY Sge (nova Sge 1783; Shara & Moffat 1983; Shara et al. 1984) is still transferring mass at a substantial rate (Somers, Mukai & Naylor 1996). DN behaviour (and hence lower mass accretion rate) is observed in the 2000-yr-old novae Z Cam (Shara et al. 2007, 2012a) and BK Lyn (Patterson et al. 2013). There has not been, until now, a nova which 'bridged the gap' between two centuries and two millennia. AT Cnc is now established as that nova. It demonstrates that 240–465 yr after it erupted as a CN, it has become a low mass-transfer rate DN.

Finally, we note that the deduced eruption date – 1686 CE, with an error of roughly one century in either direction, is in remarkable agreement with a 'guest star' reported by Korean observers in 1645 CE in the asterism Yugui (part of the constellation Cancer) (Xi & Po 1966). Warner (2015) notes the same coincidence, as pointed out by Nickiforov (2010). We discuss this guest star in an appendix.

5 CONCLUSIONS

We have measured the radial velocities of 100 blobs in the ejecta of the old nova (and currently DN) AT Cnc. The fastest moving blobs have velocities of 475 km s^{-1}. Combined with the observed angular size of the ejecta, and the distance to AT Cnc, we have determined that the CN which generated the ejecta occurred 330^{+135}_{-90} yr ago. It is the best determined transition time, to date, for an old nova to become a DN. It is also consistent with the cooling time of a WD after a CN eruption, and the time-scale predicted by the hibernation scenario of CBs for mass transfer to decline substantially after a CN eruption. The deduced date of AT Cnc's nova eruption (within a century of 1686 CE) is remarkably close in time and location to a 'guest star' reported by Korean observers in Cancer in 1645 CE. We discuss this further in Appendix B.

ACKNOWLEDGEMENTS

Based on observations obtained with SITELLE, a joint project of the Université Laval, ABB, Université de Montréal, and the CFHT, which is operated by the National Research Council (NRC) of Canada, the Institut National des Science de l'Univers of the Centre National de la Recherche Scientique (CNRS) of France, and the University of Hawaii. LD is grateful to the Natural Sciences and Engineering Research Council of Canada, the Fonds de Recherche du Québec, and the Canada Foundation for Innovation for funding. We thank Dave Zurek for help in retrieving and understanding earlier images of AT Cnc.

REFERENCES

Brousseau D., Thibault S., Fortin-Boivin S., Zhang H., Vallée P., Auger H., Drissen L., 2014, in Ramsay S. K., McLean I. S., Takami H., eds, Proc. SPIE Conf. Ser. Vol. 9147, Ground-based and Airborne Instrumentation for Astronomy V. SPIE, Bellingham, p. 91473Z
Chen H.-L., Woods T. E., Yungelson L. R., Gilfanov M., Han Z., 2016, MNRAS, 458, 2916
Chesneau O. et al., 2012, A&A, 545, A63
Cohen J. G., 1985, ApJ, 292, 90
Collazzi A. C., Schaefer B. E., Xiao L., Pagnotta A., Kroll P., Löchel K., Henden A. A., 2009, AJ, 138, 1846
Domínguez A. et al., 2013, ApJ, 763, 145
Downes R. A., Duerbeck H. W., 2000, AJ, 120, 2007
Drissen L., Rousseau-Nepton L., Lavoie S., Robert C., Martin T., Martin P., Mandar J., Grandmont F., 2014, Adv. Astron., 2014, 293856
Duerbeck H. W., 1987, Ap&SS, 131, 461
Gill C. D., O'Brien T. J., 1999, MNRAS, 307, 677
Grandmont F., Drissen L., Mandar J., Thibault S., Baril M., 2012, in McLean I. S., Ramsay S. K., Takami H., eds, Proc. SPIE Conf. Ser. Vol. 8446, Ground-based and Airborne Instrumentation for Astronomy IV. SPIE, Bellingham, p. 84460U
Harman D. J., O'Brien T. J., 2003, MNRAS, 344, 1219
Kovetz A., Prialnik D., Shara M. M., 1987, Ap&SS, 131, 419
Kozhevnikov V. P., 2004, A&A, 419, 1035
Martin T., Drissen L., Joncas G., 2015, in Taylor A. R., Rosolowsky E., eds, ASP Conf. Ser. Vol. 495, Astronomical Data Analysis Software and Systems XXIV. Astron. Soc. Pac., San Francisco, p. 327
Martin T., Prunet S., Drissen L., 2016, MNRAS, 463, 4223
Matteucci F., Renda A., Pipino A., Della Valle M., 2003, A&A, 405, 23
Nickiforov M. G., 2010, Bulg. Astron. J., 13, 116
Nogami D., Masada S., Kato T., Hirata R., 1999, PASJ, 51, 115
Oort J. H., 1946, MNRAS, 106, 159
Osaki Y., 1974, PASJ, 26, 429
Patterson J. et al., 2013, MNRAS, 434, 1902
Prialnik D., Shara M. M., 1986, ApJ, 311, 172
Prialnik D., Shara M. M., Shaviv G., 1978, A&A, 62, 339
Shara M. M., Moffat A. F. J., 1983, ApJ, 264, 560
Shara M. M., Moffat A. F. J., McGraw J. T., Dearborn D. S., Bond H. E., Kemper E., Lamontagne R., 1984, ApJ, 282, 763

Shara M. M., Livio M., Moffat A. F. J., Orio M., 1986, ApJ, 311, 163
Shara M. M. et al., 2007, Nature, 446, 159
Shara M. M., Mizusawa T., Zurek D., Martin C. D., Neill J. D., Seibert M., 2012a, ApJ, 756, 107
Shara M. M., Mizusawa T., Wehinger P., Zurek D., Martin C. D., Neill J. D., Forster K., Seibert M., 2012b, ApJ, 758, 121
Somers M. W., Mukai K., Naylor T., 1996, MNRAS, 278, 845
Starrfield S., Truran J. W., Sparks W. M., Kutter G. S., 1972, ApJ, 176, 169
Stephenson F. R., Green D. A., 2002, Historical Supernovae and Their Remnants, Vol. 5. Clarendon Press, Oxford
Taylor G., 1950, Proc. R. Soc. A, 201, 159
Warner B., 2015, hasa.conf, p. 2. Available at: http://pos.sissa.it/cgi-bin/reader/conf.cgi?confid=241
Xi, Ze-zong, Po, Shu-jen1966, Science, 154, 597
Yaron O., Prialnik D., Shara M. M., Kovetz A., 2005, ApJ, 623, 398

SUPPORTING INFORMATION

Supplementary data are available at *MNRAS* online.

Video 1

Please note: Oxford University Press is not responsible for the content or functionality of any supporting materials supplied by the authors. Any queries (other than missing material) should be directed to the corresponding author for the paper.

APPENDIX A: A SPECTRUM OF THE DWARF NOVA

The Hα emission line of AT Cnc is sometimes observed to be in emission, sometimes in absorption, and occasionally a P Cygni profile is detected. In Fig. A1, we show the spectrum of the central binary in AT Cnc, extracted from the data cube. It clearly shows Hα in emission, about twice as strong as the nebular lines in the blobs; after correction for the instrumental line function, it corresponds to a- full width at half-maximum (FWHM) of $\sim$400 km s^{-1}, centred on a velocity of +24 km s^{-1}. The modest FWHM suggests that we are seeing the accretion disc nearly face-on, consistent with our interpretation of the highest velocity ejected blobs belonging to polar caps. There is also a hint of the He I λ6678 in emission, as well as a broad absorption at 650 nm.

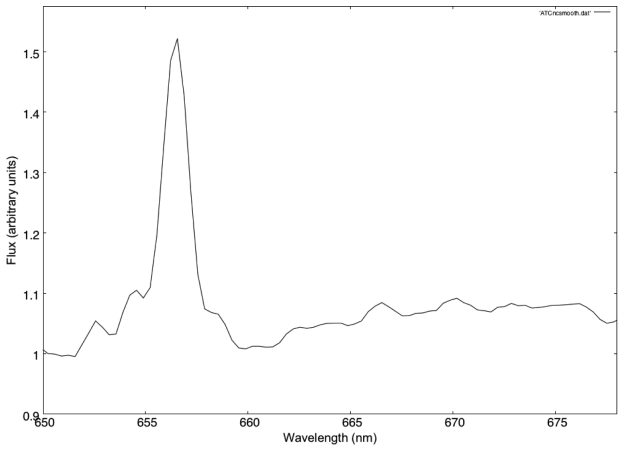

Figure A1. Spectrum of AT Cnc, smoothed with a 0.5-nm kernel.

APPENDIX B: A 'GUEST STAR' IN CANCER IN 1645 CE

A 'guest star' is mentioned in chapter 6 of the Korean encyclopedia entitled 'Chungbo Munhon Pigo' (='revised encyclopedia'). This work, which was compiled in 1907, was a revision of a work compiled in 1770. The complete entry relating to the star gives only the year (23rd year of King Injo) and lunar month – the second month. The precise date are not given; the Julian Date is thus equivalent to some time between CE 1645 February 26 and March 27). The record simply states that 'a large star (daxing) entered (ru) Yugui'. The duration of visibility is not specified.

The star group Yugui, in Cancer, consisted of the four stars theta, eta, gamma, and delta Cnc. The northernmost star of Yugui, gamma Cnc, is located at a declination of +21°28′, nearly 4° south of AT Cnc. The brief text only mentions Yugui but does not use the expression xiu ('lunar lodge'). This suggests that the small and well-defined star group Yugui in Cancer, rather than the much larger lunar lodge, covering much of Cancer, and including AT Cnc, was intended.

The Chungbo Munhon Pigo is not a very reliable source. For instance, it falsely records 'guest stars' in both AD 1600 and 1664, which, as comparison with the more detailed Sillok ('Veritable Records') reveals, were misplaced entries of the supernova of AD 1604 (Stephenson & Green 2002, pp. 70–71). A similar error might have occurred around AD 1645.

To search for more potential information, co-author F. Richard Stephenson has carefully checked the Korean chronicle known as the Injo Sillok ('Veritable records of the reign of King Injo'), a detailed day-to-day chronicle. It is mainly concerned with non-astronomical matters, but from time to time, there are entries of astronomical interest. A search of the chronicle for the first and second months of the 23rd year of King Injo reveals 10 reports of astronomical events – such as conjunctions of the Moon with stars, eclipses, etc., over these two months. There is no reference to a guest star seen at Yugui.

An alternative interpretation is that the 'large star', said to 'enter' Yugui, might have been a comet. However, there are no known records of either guest stars or comets in Chinese history for AD 1645. As this was only the second year of the Qing dynasty after the defeat of the Ming in 1644, records may be incomplete in this turbulent period.

In summary, while the fragmentary Korean record of a transient in the southern part of the constellation Cancer in 1645 CE is in intriguing proximity, both in time and location, to our deduced date of the last nova eruption of AT Cnc, the evidence currently available is insufficient to support a claim of a likely coincidence.

This paper has been typeset from a TEX/LATEX file prepared by the author.